Clinical, Cosmetic and Investigational Dermatology

Dovepress

open access to scientific and medical research

Open Access Full Text Article

ORIGINAL RESEARCH

Integrated Analysis Reveals COL4A3 as a Novel Diagnostic and Therapeutic Target in UV-Related Skin Cutaneous Melanoma

Zuochao Yao, Lu Lu, Qianhui Xu, Shan Hua, Hui Wang, Hua Jiang

Department of Plastic and Reconstructive Surgery, Shanghai East Hospital, School of Medicine, Tongji University, Shanghai, 200092, People's Republic of China

Correspondence: Hui Wang; Hua Jiang, Department of Plastic and Reconstructive Surgery, Shanghai East Hospital, School of Medicine, Tongji University, 150 Jimo Road, Pudong New Area, Shanghai, 200092, People's Republic of China, Email pathology2000@163.com; jianghua@tongji.edu.cn

Background: High levels of UV exposure are a significant factor that can trigger the onset and progression of SKCM. Moreover, this exposure is closely linked to the malignancy of the tumor and the prognosis of patients. Our objective is to identify a tumor biomarker database associated with UV exposure, which can be utilized for prognostic analysis and diagnosis and treatment of SKCM.

Methods: This study used the weighted gene co-expression network analyses (WGCNA) and gene mutation frequency analyses to screen for UV-related target genes using the GSE59455 and the cancer genome atlas databases (TCGA). The prognostic model was created using Cox regression and least absolute shrinkage and selection operator analyses (LASSCO). Furthermore, in vitro experiments further validated that the overexpression or knockdown of COL4A3 could regulate the proliferation and migration abilities of SKMEL28 and A357 melanoma cells.

Results: A prognostic model was created that included six genes with a high UV-related mutation in SKCM: COL4A3, CHRM2, DSC3, GIMAP5, LAMC2, and PSG7. The model had a strong patient survival correlation ($P<0.001$, hazard ratio (HR) = 1.57) and significant predictor ($P<0.001$, HR = 3.050). Furthermore, the model negatively correlated with immune cells, including $CD8^+$ T cells (Cor=−0.408, $P<0.001$), and M1-type macrophages (Cor=−0.385, $P<0.001$), and immune checkpoints, including programmed cell death ligand-1. Moreover, we identified COL4A3 as a molecule with significant predictive functionality. Overexpression of COL4A3 significantly inhibited the proliferation, migration, and invasion abilities of SKMEL28 and A357 melanoma cells, while knockdown of COL4A3 yielded the opposite results. And overexpression of COL4A3 enhanced the inhibitory effects of imatinib on the proliferation, migration, and invasion abilities of SKMEL28 and A357 cells.

Conclusion: The efficacy of the prognostic model was validated by analyzing the prognosis, immune infiltration, and immune checkpoint profiles. COL4A3 stands out as a novel diagnostic and therapeutic target for SKCM, offering new strategies for small-molecule targeted drug therapies.

Keywords: prognostic model, skin cutaneous melanoma, SKCM, the weighted gene co-expression network analysis, WGCNA, immune cell infiltration, mutation

Introduction

Melanoma is a malignant tumor that develops from epidermal melanocytes and has a poor prognosis due to its extreme aggressiveness and resistance to treatment.[1] The importance of gene mutations in cancer metastasis cannot be overestimated. Skin cutaneous melanoma (SKCM) is sensitive to deoxyribonucleic acid (DNA) changes.[2] Moreover, some studies have identified mutations in driver genes, including BRAF and NRAS, as the most probable pathogenic mechanism, allowing faulty cells to survive and infiltrate tissues.[3] Most melanoma mutations are linked to ultraviolet (UV) exposure. High-energy UV causes cytosine dimer (CC) formation by generating oxygen radicals. Furthermore, the CC frequently mismatches with two adenines during DNA replication, increasing the fragility of the DNA helix structure and, eventually, the classic UV-mediated CC→ thymine dimer (TT) mutation.[4] Some studies have discovered that exposure to UVB (280–320 nm) light in sunlight, closer to the absorption peak of nucleotides, can cause DNA alterations

Received: 6 March 2024
Accepted: 7 May 2024
Published: 17 June 2024

in approximately 10–15 min.[5] In conclusion, these results also imply that UV-induced alterations can cause SKCM to invade and metastasize more actively.

UV radiation not only possesses genotoxicity but also impacts the occurrence and progression of melanoma from multiple perspectives, including the tumor immune microenvironment and drug resistance.[6,7] The immune microenvironment is a crucial factor influencing the proliferation and migration of tumors. Previous studies have indicated that UV exposure can induce highly invasive melanoma and reduce tumor heterogeneity. This change in heterogeneity is not dependent on genetic mutations but is an independent risk factor associated with the tumor's immune microenvironment.[8] Similarly to the oncogenic genes BRAF and NRAS, which directly modulate the cell cycle and apoptosis through the PI3K/AKT pathway, they are also identifiable by the immune system, prompting the activation of antitumor immune responses against novel antigens.[9] Hence, the alterations in the microenvironment induced by UV exposure are equally pivotal. The resistance of tumors, also induced by UV exposure, poses a significant and undeniable challenge.[10] Researchers have reported an increase in the activity of histone deacetylase 8 (HDAC8) induced by UV, along with MAPK and AP-1 signaling, resulting in the development of a drug-resistant phenotype in melanoma.[11] Conversely, the inhibition of tumor suppressor genes or proteins can also facilitate the promotion of tumor occurrence and progression by UV.[12] This suggests that UV can influence the drug resistance of melanoma by modulating protein expression levels and affecting protein activity.

Currently, research on genes associated with UV-induced mutations is limited. There is also a lack of investigation into identifying targets within these genes that could impact the prognosis and drug sensitivity of SKCM. This study employed bioinformatics analysis to identify a high-frequency hub of genes associated with UV exposure. A predictive model for forecasting the prognosis of SKCM patients was constructed based on these findings. This model can be utilized to predict the immune microenvironment and the responsiveness to immune checkpoint inhibitors in SKCM patients. Furthermore, we identified a key molecule COL4A3, which can regulate the vitality of human melanoma cells and is associated with the therapeutic efficacy of the chemotherapy targeting drug imatinib. These findings will contribute to the formulation of personalized treatment plans for SKCM patients, enhance treatment targets, and ultimately improve their disease outcomes.

Methods

Obtaining the Differentially-Expressed Genes (DEGs) in SKCM

Based on the ribonucleic acid (RNA) sequencing of GSE59455, differential genes were calculated in patients with primary melanoma (n=39) and patients with metastatic melanoma (n=102) using the limma package in R software (version 3.4.0, https://www.r-project.org/). Statistical significance was set at an adjusted $P < 0.05$ and the absolute log2 fold change (log2FC) > 1. The cBioPortal (www.cbioportal.org)[13] and Oncomine (www.oncomine.org)[14] databases were used to assess the expression of DEGs in SKCM cells. The cancer genome atlas (TCGA) gene alterations (mutations and copy number changes) and gene expression (reads per kilobase of RNA-Seq reads) of the dataset were analyzed using the cBioPortal software with the default settings. Immunohistochemical images of skin tissues were acquired through the human protein atlas database.

Weighted Gene Co-Expression Network Analysis (WGCNA) for Calculating UV-Related Scores Module

DEGs acquired from GSE59455 and the clinical characteristics presented in this dataset, particularly the solar elastosis and possible sun exposure scores linked with UV, were inputted simultaneously into the WGCNA.[15] First, using the R package "WGCNA", the soft threshold parameters $\beta=5$ and scale-free $R^2=0.90$ were computed and set. Subsequently, the input DEGs were categorized into distinct gene modules based on the similarity of expression patterns, yielding a gene co-expression matrix. The heat map displays these distinct connections after calculating the correlations between these module Eigengenes and clinical features using the Eigengenes algorithm. This module was identified as the turquoise module having the highest correlation with the solar elastosis score. Finally, the relationship between the solar elastosis score and specific module genes was computed and presented as scatter plots.

Enrichment Analysis

Gene Ontology and Kyoto Encyclopedia of Genes and Genomes pathway enrichment analyses were performed on 815 genes of the turquoise module using the DAVID (https://david.ncifcrf.gov/) to analyze the biological processes, cellular components, molecular functions, and pathways affected by UV-related module gene hub. These results were presented as bubble plots. The molecules were graded based on the log2 FC values of DEGs to assess whether they were enriched in a set of genes. Additionally, gene set enrichment analysis (GSEA) pathways from the molecular signatures database (http://software.broadinstitute.org/gsea/msigdb) [16] have been predefined.

Construction and Validation of Prognostic Models

Multifactorial Cox regression and least absolute shrinkage and selection operator (LASSO)[17] analysis was used to develop prognostic models. In this study, we use the LASSO regression algorithm to build a stable model and screen for prognosis-related genes with high accuracy. LASSO models for the top 20 UV-related prognostic genes with mutation rates were created using the R software, and the risk score composition for prognosis was as follows:

Risk score = (β_1 * gene 1 expression level) + (β_2 * gene 2 expression level) +……+ (β_n * gene n expression level).

The median survival information of patients with SKCM from the TCGA database was used to categorize patients into high-risk and low-risk groups. The importance of prognostic risk score and clinical features in predicting survival outcomes was determined using univariate Cox regression analysis with a cutoff value of $P<0.05$. Significance factors were evaluated using multivariate Cox regression analysis, followed by statistical nomogram analysis using the R software to eliminate confounding factors. The Wilcoxon signed-rank test was used to compare the expression of six important genes in primary and metastatic tumor tissues. Furthermore, Kaplan–Meier curves were utilized to assess the prognostic model's prediction ability and receiver operating characteristics (ROC) curve analysis.

Calculating the Correlation Between Immune Infiltration and Prognostic Models

The sample of SKCM whole transcriptome messenger RNA data was processed and transformed into an absolute abundance of immune and stromal cell types in diverse tissues using the R package "CIBERSORT"[18] of R software to mimic the extent of infiltration of 22 immune cell subpopulations in human. After organizing gene expression profiles using standard annotation files, correlations between the risk score of the built prognostic models and the degree of immune cell infiltration were obtained, and heat maps were created. We also investigated 11 common immune checkpoints in tumor sample species, including PD-1, and computed and illustrated their association with the model. To further illustrate the importance of COL4A3 for melanoma metastasis and prognosis, we included The University of Alabama at Birmingham Department of Pathology (UALCAN) Database (https://ualcan.path.uab.edu/tutorial.html) and The Gene Expression Profiling Interactive Analysis (GEPIA) (http://gepia.cancer-pku.cn/index.html), and perform KM survival curve analysis.

Construction and Assessment of a Predictive Nomogram

Based on univariate and multifactorial regression analyses, independent analysis of the prognostic predictive power of factors such as TNM stage, age, and risk score of patients with tumors. Using R software, the nomogram column line and corresponding calibration plots were constructed by integrating factors with apparent predictive efficacy. The specificity of the predictive power of the column line graphs and the risk score as independent risk factors was assessed by plotting ROC curves. Finally, decision curve analysis was used to evaluate the clinical benefit of the column line graphs compared to a single independent prediction.

Correlation Analysis of Chemotherapy and Small Molecule Drugs

The response to chemotherapy medications in patients with SKCM was predicted using the Genomics of Drug Sensitivity in Cancer (GDSC) database (www.cancerRxgene.org).[19] It encompasses vast datasets on drug sensitivity and genomics, aiding the exploration of new therapeutic biomarkers for cancer treatment. To identify SKCM sensitive drugs associated with the biomarkers we screened, the "predict" package of the R software was used to determine the half-maximal

inhibitory concentration and gauge the patient's reaction to chemotherapeutic drugs. A connection map is a database of biological applications that combines diseases, gene expression, and small-molecule medications. By analyzing the expression of type IV collagen alpha 3 chain (COL4A3), it is possible to identify the drugs associated with it that stimulate or reverse the biological process of the tumor.

Cell Culture and Transfection

The human skin melanocyte line A357 and SKMEL28 were purchased from Wuhan Pnoxel Biological Company, Wuhan, China, and cultured using DMEM or RPMI-1640 medium containing 10% fetal bovine serum (supplemented with penicillin (100 U/mL) and streptomycin (100 mg-mL) (Gibco; Thermo Fisher Scientific). Cultures were performed in a cell incubator at 37°C, 5% CO_2.

Cell transfection reagent Lipo2000 was used to complete the transfection of cell-specific small interfering RNA (si-RNA) fragment of COL4A3 (designed and synthesized by JiMan Biotechnology Shanghai Co., Ltd.), and the sequence of Si-RNA was 5'-GGGTAATCCTGGATTTCTA-3'. In addition, the RNA expression of COL4A3 in cells was detected using reverse transcription-quantitative (RT-q) after transfection to determine the efficiency. The COL4A3 (Gene ID: 1285 NC_000002.12) plasmids were subcloned into the Ubi-MCS-3FLAG-SV40-EGFP-IRES-puromycin eukaryotic expression vector (Biovector NTCC Inc.).

Western Blotting Analysis

Cells were lysed in RIPA buffer (Epizyme, Shanghai) with protease inhibitor (CoWin Biosciences, China) and phosphatase inhibitors (CoWin Biosciences, China) on ice. Samples were quantitated with BCA Protein Assay Kit (ThermoFisher, USA) measured at a wavelength of 562 nm (MD VersaMax, USA). According to the manufacturer's recommended protocol, protein samples were loaded into 7.5%-12.5% gels (Beyotime, China). After electrophoresis, proteins were transferred onto a 0.2-μm PVDF membranes (ThermoFisher, USA). After blocking the membrane with 5% non-fat milk in 1x TBS-T (Sigma, Germany), the PVDF membrane was incubated with the corresponding primary antibody for more than 12 h at 4°C, and incubated with the secondary antibody for 1 h at room temperature, and the protein bands were detected by chemiluminescence (Tanon, China). Rabbit anti- COL4A3 (Abclonal, A16359, 1:1000), rabbit anti-BCL-2 (Abclonal, A19693, 1:1000), rabbit anti Cleaved Caspase 3 (Abclonal, A19654, 1: 10,000), and rabbit anti-GAPDH (Proteintech, 60,004-1-Ig, 1: 10,000).

Cell Proliferation Viability Assay

Cell proliferation viability after the si-RNA intervention was assayed using the Cell Counting Kit-8 (CCK-8) assay (Beyoncé) and EdU (Beyoncé) according to the manufacturer's instructions. SK-MEL-28 was inoculated into 96-well plates at a cell density of 10^5 pcs/cm^2. After the cells were plastered, incubation was continued in a constant temperature incubator for 0, 12, 24, and 48 h immediately, and 10 μL of CCK-8 reagent was added to each well, respectively, and incubation was continued for 3 h. The change in colorimetric intensity was quantified by measuring the optical density of formazan salt at 450 nm by a microplate reader (Molecular Devices Inc., USA). Five sample replicate wells were set up for each group in the experiment.

Wound-Healing Assay

SK-MEL-28 cells were inoculated into 6-well plates at 2×10^5 per well, and si-RNA was transfected into the cells after the cells were walled up to determine the COL4A3 effect on the migratory capacity of SK-MEL-28 cells. When the cell density reached 90–100%, the cell colonies were scratched along a straight line using the tip of a 200 μL pipette. The medium was removed, and the cells were gently rinsed with phosphate-buffered saline. Subsequently, the cells were replaced with RPMI-1640 medium containing 1% fetal bovine serum. Images were captured at the scratch site under a light microscope at 0, 12, and 24 h after scratching the cells, and the wound area was determined. Further, the wound healing rate was calculated and counted for different groups simultaneously. At least three replicate groups were set up for each experiment group.

Transwell Invasion Assay

The transwell chambers was used for assessing the cell migration. The cells were seeded in serum-free medium of the Matrigel-precoated upper-side of chambers (BD Biosciences, USA). The bottom chambers were added with the serum-free

medium containing DMEM without FBS as a chemoattractant. After 24 h, a cotton swab was employed for removing the residual non-invasive cells in the upper side of chambers. The cells moved to the low side of chambers were fixed with 100% methanol, then stained with 0.5% crystal violet. The transwelled cells were pictured under the inverted microscope.

Statistical Analyses

R (version 3.40) and GraphPad Prism 7 tools were used for statistical analysis and graph production (version 7.0). The Student's *t*-test was used to assess differences in normally distributed data across paired groups. The Kaplan-Meier technique and Log rank test were used for survival analysis. The Wilcoxon rank sum test was used to compare the differences between the two groups in non-normally distributed data, and the findings were reported as medians (interquartile difference). Statistical significance was defined as $P<0.05$.

Results

Identifying UV-Related Gene Modules Using WGCNA

To elucidate the connection between UV-induced mutated genes and SKCM transfer viability, it is essential to identify Differentially Expressed Genes (DEGs) between primary and metastatic tumors. In the initial analysis, the complete transcriptome expression sequencing matrix from the GSE59455 dataset was employed, resulting in the identification of 2862 DEGs across 39 patients with primary melanoma and 102 patients with metastatic melanoma.

The soft threshold value $\beta=5$ was computed and selected using the R package "WGCNA". Clustering analysis was then performed by integrating specified parameters and the expression pattern of DEGs to generate a gene co-expression matrix, resulting in the identification of 10 distinct gene modules. Figure 1A and B illustrate the results of soft threshold selection and clustering analysis. In assessing UV-related exposure, crucial factors in melanoma development for patients include the solar elastosis score and the sun exposure score. Subsequently, the correlation between all modules and clinical features is depicted (Figure 1C). Notably, the sun exposure score exhibited a positive correlation with the gene module. The UV-related gene module, specifically the turquoise module, demonstrated the strongest connection with the sun exposure score (Cor=0.61, $P<0.001$). Finally, through a scatter plot (Figure 1D), illustrates the fitting of the 815 individual genes in the module to the sun exposure score, revealing a significant linear dependence.

UV-Related Gene Module Enrichment and Construction of Prognostic Model

To enhance the elucidation of the functions of the differentially expressed genes within the selected turquoise module, we conducted further biogenic analysis on them. Figure 2A depicts the findings of the UV-related module's 815 genes used for gene ontology (GO) and Kyoto Encyclopedia of Genes and Genomes analyses (KEGG), with the top 12 enriched items occupying most of them, such as keratinocyte differentiation and skin development. The primary findings of GSEA analysis also focused on skin growth following the log2FC values (Figure 2B). Moreover, the DNA Repair pathway and Cell Cycle pathway were found to be enriched, signifying that these genes effectively capture the damage and alterations induced by UV exposure.

Utilizing survival data from 472 patient samples in TCGA database, we employed Cox regression analysis to identify 4489 genes associated with prognosis, among which 151 key genes were concurrently present in the turquoise module gene set. These 151 key genes, validated across multiple datasets, are implicated in UV-related prognosis in SKCM. Subsequently, we integrated mutation information from 480 melanoma cell samples, constructing a mutation spectrum for the 151 genes in SKCM (Figure 2C). Supplementary Figure 1 presents the overall view of all 151 genes mutation frequencies.

Among the top 30 genes, there was a mutation rate of approximately 5% or more in the samples, with the top 11 genes exhibiting a significant mutation rate exceeding 10%. We selected the top 20 genes with mutation rates and used the LASSO method to fit and screen six of the 20 genes with more prominent performance, namely CHRM2, COL4A3, DSC3, GIMAP5, LAMC2, and PSG7. The prognostic model based on these genes was built using the following formula: Risk score =−0.0226393876358178*log2(CHRM2) - 0.262085087886837*log2(COL4A3) + 0.0621140046143123*log2(DSC3) - 0.179580917149916*log2(GIMAP5) + 0.0675711299725153*log2(LAMC2) + 0.43414244015*log2(PSG7) (Figure 2D and E) (Table 1). Figure 2F and G illustrate the risk score and sample survival for each sample of this model.

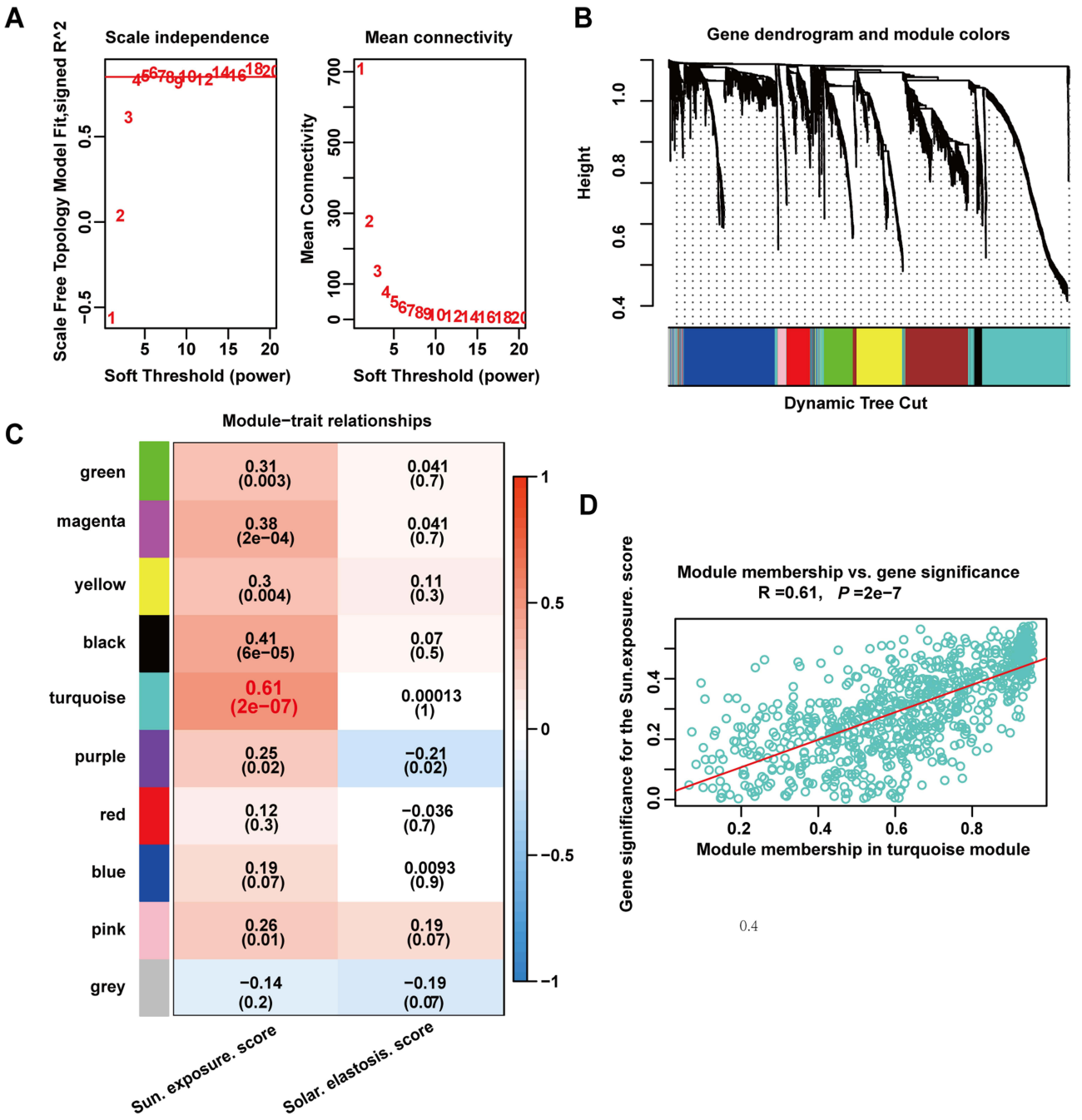

Figure 1 Identifying UV-related gene modules using WGCNA. (**A**) Soft threshold (β) analysis and selection; (**B**) A dendrogram of all differentially expressed genes grouped according to a dissimilarity metric was created (1-TOM); (**C**) A heatmap depicting the relationship between module eigengenes and UV-related clinical features; (**D**) The module significance of the turquoise module.

Construction and Validation of a Nomogram Integrating Risk Score

Using the prognostic model, each melanoma sample in the TCGA dataset was classified and grouped based on the median. Kaplan-Meier analysis revealed that the low-risk group (n=227) exhibited significantly better overall survival (OS) and disease-specific survival (DSS) outcomes compared to the high-risk group (n=227) (Figure 3A–D). The survival ROC curve areas under the curve at 1 year, 2 years, and 3 years were 0.610, 0.605, 0.611, and 0.59, 0.601, 0.588, respectively. Subsequently, clinical data (including age, weight, sex, and tumor TNM stage) from patients with SKCM in the TCGA were analyzed using univariate and multifactorial regression analyses to assess the independent

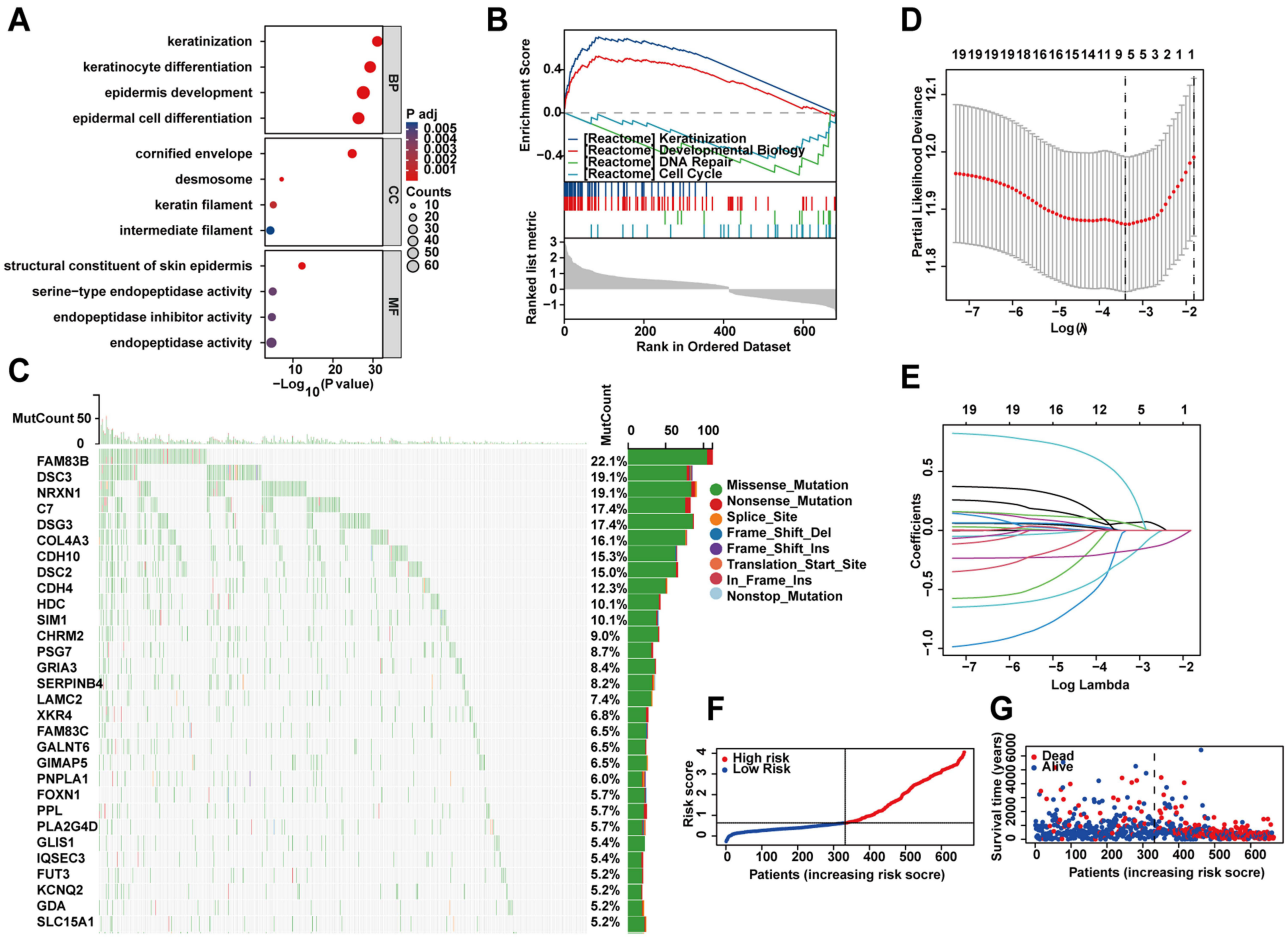

Figure 2 Module enrichment and construction of the prognostic model. (**A**) UV-related gene modules are enriched in the GO and KEGG items shown in the bubble map; (**B**) Module enrichment analysis using GSEA; (**C**) The top 30 genes in terms of mutation frequency; (**D** and **E**) Prognostic model construction using LASSO analysis; (**F** and **G**) The risk score and sample survival for each sample of this model.

predictive role of the prognostic model on patient prognosis (Figure 3E and F). The prognostic model risk score (P<0.001, HR = 3.050), TNM stage, and age (P<0.05, HR = 1.014) were all independent predictors of SKCM prognosis. A line graph was generated using the nomogram based on these independent prognostic factors to examine the survival prediction of patients with SKCM at 1, 2, and 3 years (Figure 3G). Decision curve analysis confirmed the nomogram's ability to predict prognosis. In addition, the results suggested that it has high clinical benefit, implying that the nomogram has some practical use in clinical practice (Figure 3H–J).

Table 1 The Results of LASSO Model

	Gene ID	Description	Coefficient
CHRM2	1129	Cholinergic receptor muscarinic 2	−0.02263
COL4A3	1285	Collagen type IV alpha 3 chain	−0.26208
DSC3	1825	Desmocollin 3	0.06211
GIMAP5	55,340	GTPase, IMAP family member 5	−0.17958
LAMC2	3918	Laminin subunit gamma 2	0.06757
PSG7	5676	Pregnancy specific beta-1-glycoprotein 7	0.43414

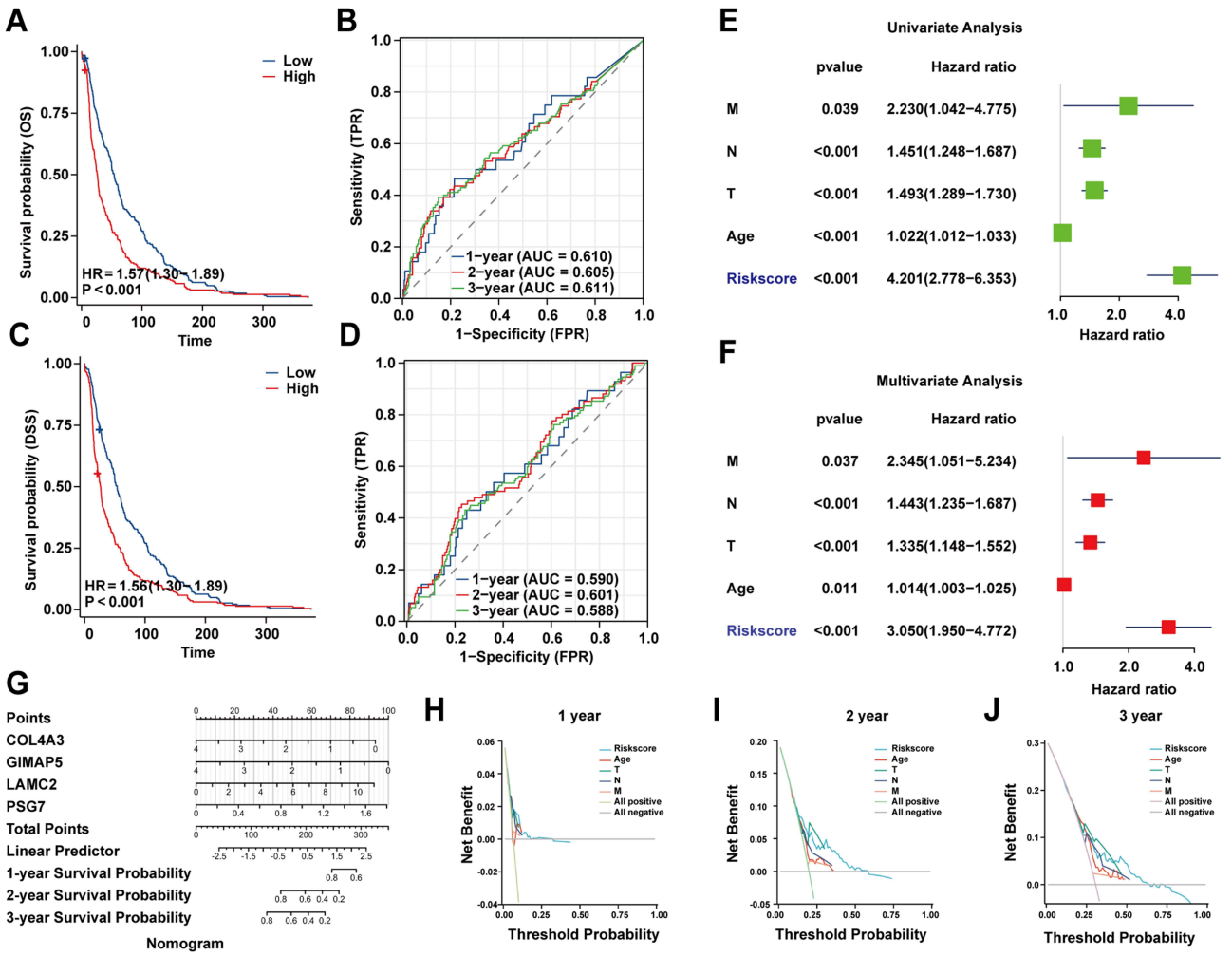

Figure 3 Validation of prognostic model. (**A**–**D**) Kaplan-Meier graphs exhibiting OS and DSS outcomes for low and high score groups, as well as ROC curves measuring validity, respectively; (**E** and **F**) Univariate and multifactorial regression analyses for the prognostic model; (**G**) The nomogram, an examination of independent risk factors that potentially predict prognosis, are displayed in columnar graphs; (**H**–**J**) Decision curve analysis (DCA) analysis confirmed nomogram's ability.

Immunological Infiltration and Immune Checkpoint Profiling Based on Risk Score

We attempted to investigate the immune infiltration and checkpoint profile of SKCM to explore further and validate the model's clinical value. Patients possessing prognostic information in the TCGA cohort were separated into high-risk and low-risk groups using the median risk score to investigate the connection between the UV-related prognostic model and immunotherapy. The ESTIMATE algorithm was used to assess the immunological levels of patients with SKCM. The low-risk score group had considerably higher ESTIMATE, immune, and stromal scores but lower tumor purity than the high-risk group (P<0.001) (Figure 4A–D).

Figure 4E depicts the results of an additional examination of the link between the risk score and the level of infiltration of 22 immune cells. The risk score showed a significant correlation with various immune cells (P<0.05), with the risk score showing a negative correlation with CD8+ T cells (Cor = −0.38, P<0.001), and M1-type macrophages (Cor=−0.31, P<0.001) (Figure 4F and G). Conversely, M2-type macrophages, which are strongly linked to a poor prognosis,[20] exhibited a positive correlation (Cor=0.25, P<0.001). Moreover, this risk score is significantly negatively correlated with 11 common immune checkpoint molecules, including Programmed Death-Ligand 1 (PD-L1), and CD28, CD86, LAIR1, and PDCD1, with correlation coefficients of −0.7, −0.74, −0.75, and −0.71, respectively (Figure 4H).

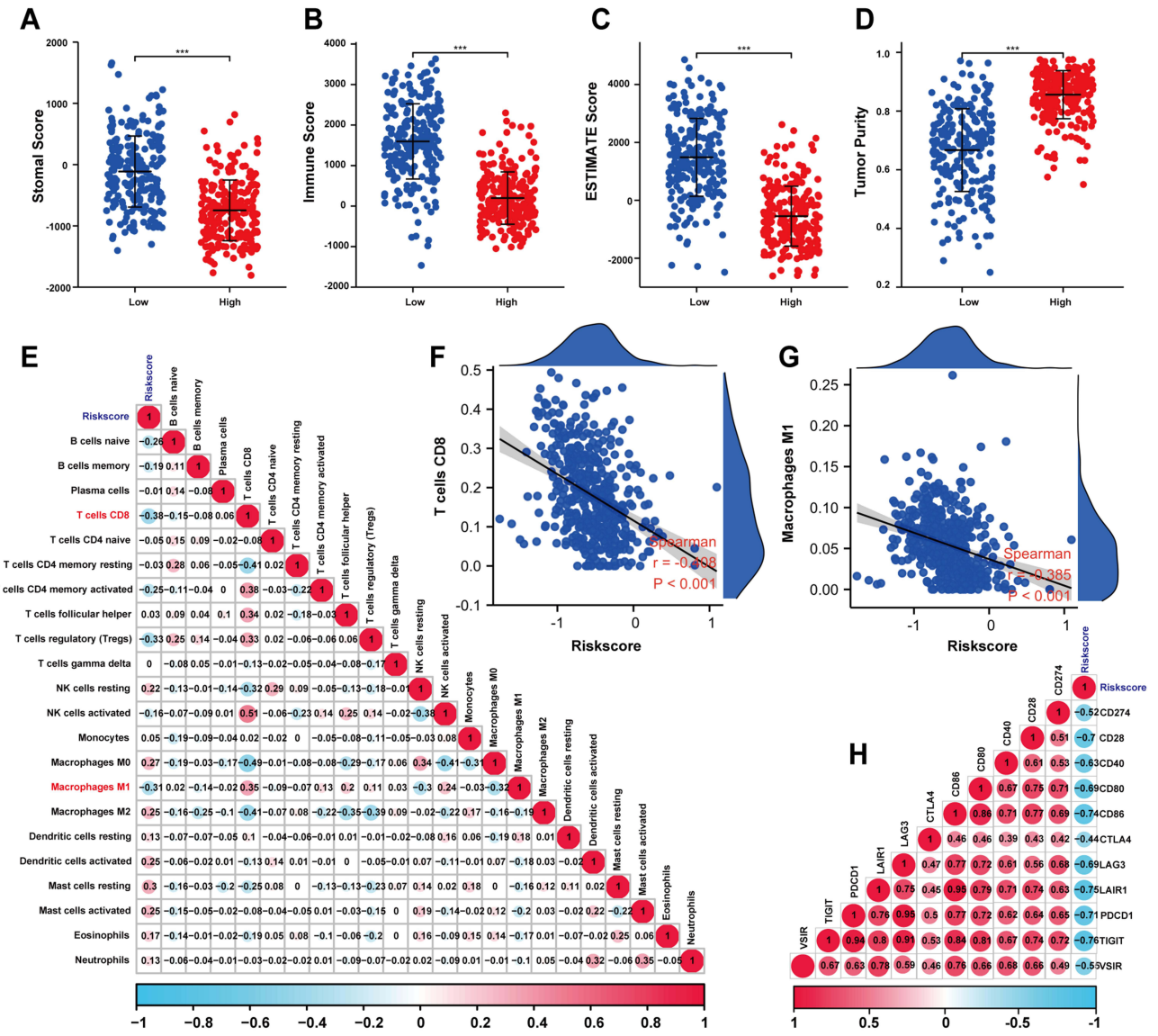

Figure 4 The correlation between immune infiltration and immune checkpoints and prognostic model. (**A–D**) The ESTIMATE algorithm for ESTIMATE scores, Immune scores, Stomal scores, and Tumor purity; (**E**) the correlation between the immune cells and prognostic risk score; (**F** and **G**) Scatter plot of the correlation between CD8+ T cells, M1-type macrophages, and risk score; (**H**) Distribution of prognostic risk score and immune checkpoint expression.

COL4A3 is an Independent Protective Factor for SKCM

COL4A3 exhibits a high mutation rate in SKCM among the six components that constitute the prognostic model. However, its role in SKCM metastasis and prognosis has been underexplored. Missense mutations of the G622E/R mutation site are the most prevalent COL4A3 mutations in SKCM (Figure 5A). Based on COL4A3 mutations, SKCM patients were divided into two groups. Subsequently, Kaplan-Meier curves were constructed to illustrate the overall survival and disease-free survival of patients in the mutated group (n=45) compared to the non-mutated group (n=321) (Figure 5B and C). The results indicate a significant association between COL4A3 mutations and overall survival for patients. Supplementary Figure 2 displays the alterations in patients' survival associated with mutations in the other five genes. These genes collectively exhibit less pronounced predictive capability compared to COL4A3.

Patients were stratified into high and low expression groups based on the median expression level of COL4A3 in SKCM samples from the TCGA database. Subsequent analysis compared the performance of TNM staging, Clark level, Breslow depth, and prognosis between the two groups (Figure 5D–G). Based on UALCAN and GEPIA Database, and perform KM survival curve analysis. The results as shown in Supplementary Figure 3, KM curve analysis based on both databases indicated

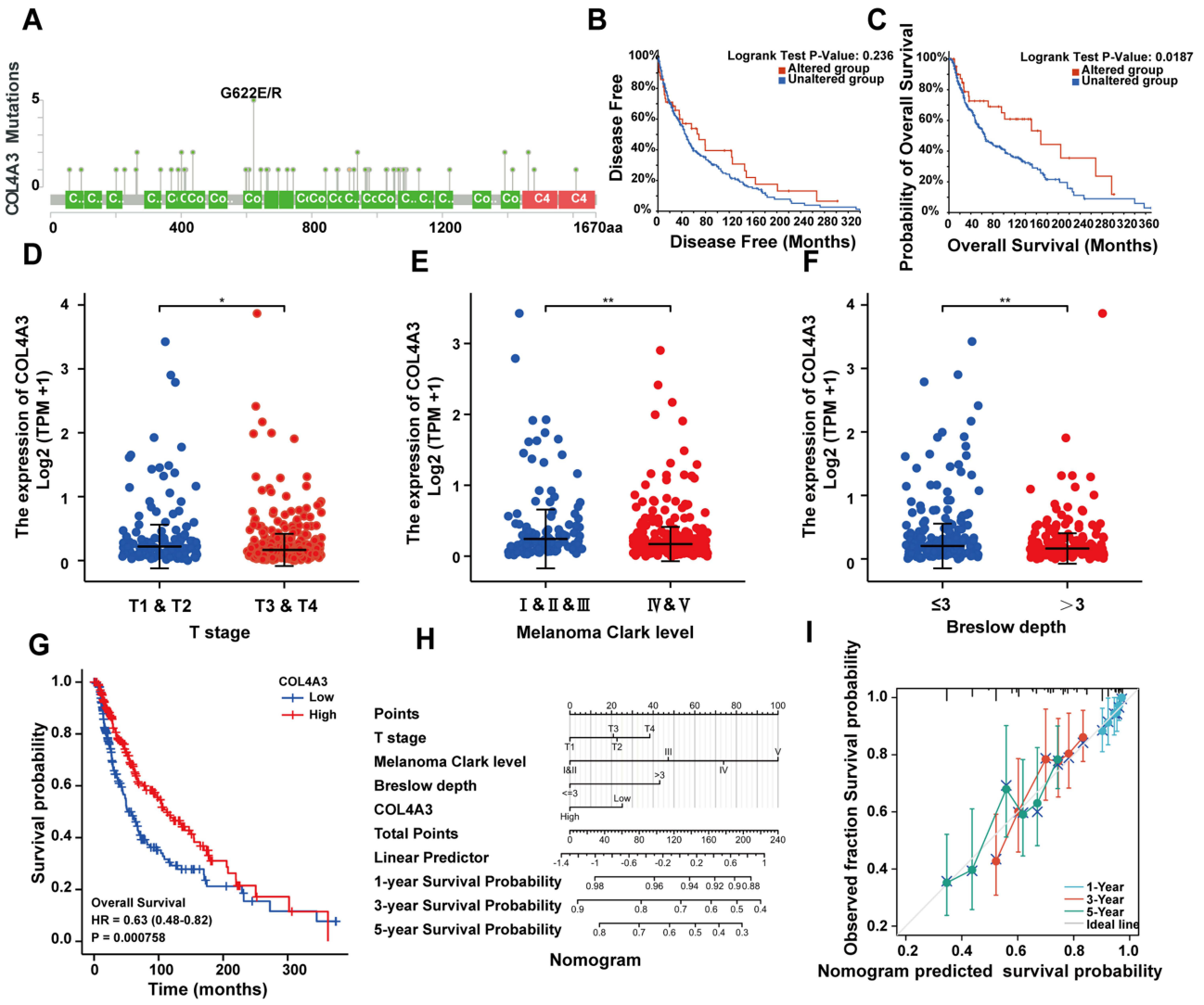

Figure 5 The prognostic analysis of COL4A3 mutation and expression in patients with SKCM. (**A**–**C**) COL4A3 mutations are related to patient survival; (**D**–**F**) Scatter plot demonstrating the relationship between COL4A3 expression and TNM staging, Clark level, and Breslow depth in SKCM; (**G**) Kaplan-Meier graphs exhibiting OS outcomes for low and high COL4A3 groups and ROC curves measuring validity; (**H** and **I**) The nomogram for potentially predicting the prognosis of COL4A3 and Calibration analysis.

that COL4A3 was significantly correlated with the prognosis of SKCM (P=0.024, P=0.00093). All findings suggest that COL4A3 is a protective factor in SKCM. And Supplementary Figure 4 Kaplan-Meier graphs exhibiting OS outcomes for low and high groups of DSC3, GIMAP5, LAMC2. Moreover, the nomogram can be utilized to estimate the risk of relapse in a patient by offering a visual representation of factors, indicating the potential use of COL4A3 as an independent risk factor at 1, 3, and 5 years (Figure 5H). Additionally, calibration analysis verified the validity of the nomogram model (Figure 5I).

Potential Correlation Between COL4A3 and Small-Molecule Targeted Drugs in SKCM

Base on drug sensitivity genomics, we predicted the correlation between COL4A3 and small-molecule chemotherapeutic drugs in SKCM patients (Figure 6A-J). The results revealed a positive correlation between COL4A3 and various clinically relevant targeted drugs for SKCM, such as imatinib (Cor=0.497, P<0.001) and dacomitinib (Cor=0.331, P=0.01). However, there is no apparent correlation with non-melanoma-targeted agents like arsenic trioxide. These findings suggest that SKCM with high COL4A3 expression may exhibit increased sensitivity to certain small-molecule targeted therapies.

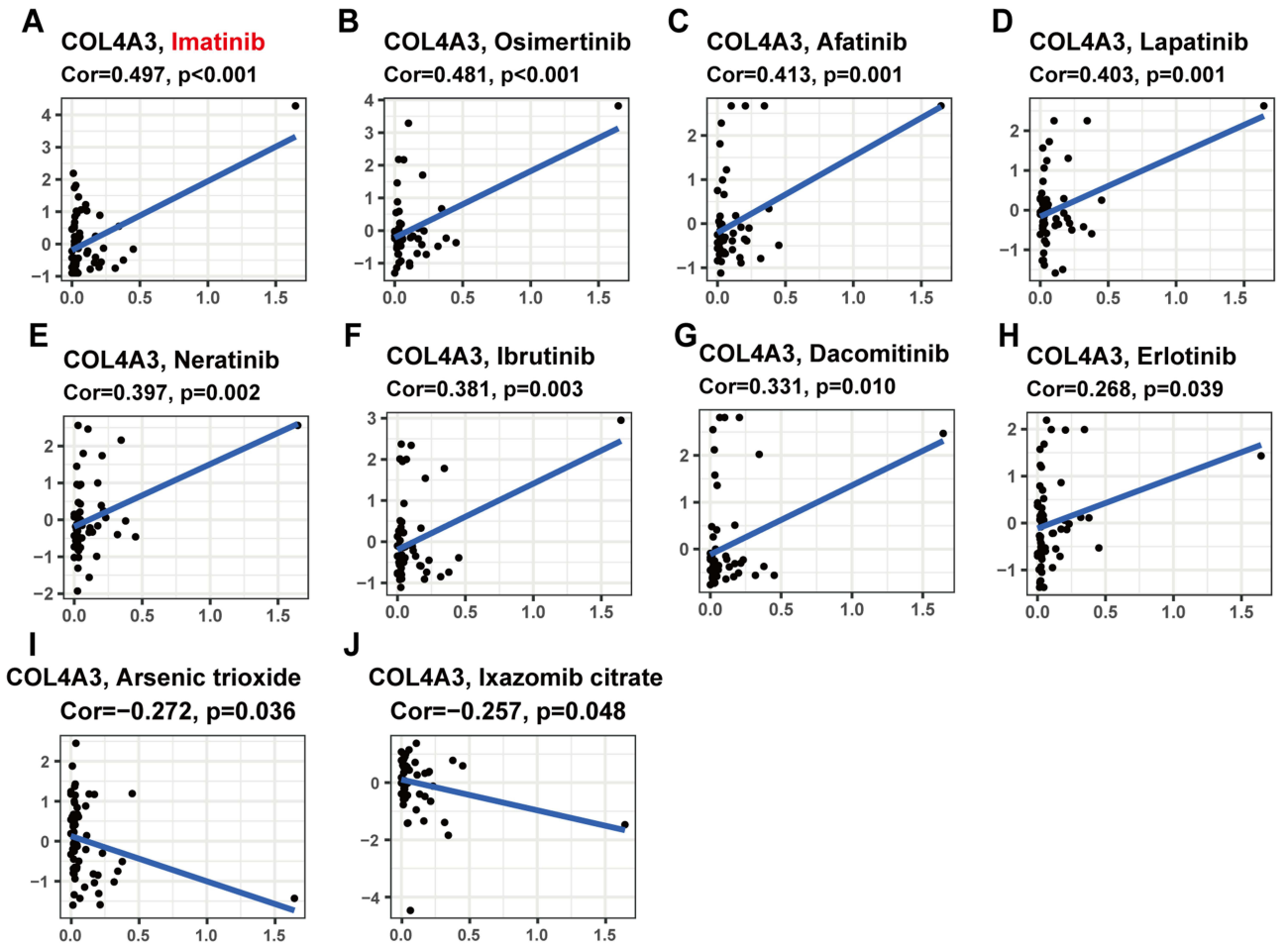

Figure 6 The response of patients with SKCM to chemotherapy drugs. (**A**–**J**) Differences in response to chemotherapy drugs between high and low expression COL4A3 patients.

The Expression of COL4A3 Can Impact the Vitality of Melanoma Cells

To further investigate whether COL4A3 indeed possesses the independently predicted protective role, A357 and SKMEL28 cells were separately transfected with Si-NC, Si-COL4A3, and pcDNA3.1-COL4A3. Initially, we examined the expression levels of COL4A3 in the control group and each transfected group through Western blot (WB) analysis. Figure 7A demonstrates the effective downregulation or overexpression of COL4A3 achieved by our constructed Si-COL4A3 and pcDNA3.1-COL4A3, respectively. Through CCK-8 assays conducted at different time points, it was observed that the proliferation of cells in the Si-COL4A3 group significantly increased compared to the Si-NC group. Conversely, the overexpression of COL4A3 resulted in the opposite outcome (Figure 7B and C). In the wound healing assay assessing cell migration capability, at the 24h and 48h time points, the healing rate in the Si-COL4A3 group was significantly faster than the control group. Conversely, the group transfected with pcDNA3.1-COL4A3 exhibited a significantly decelerated healing speed (Figure 7D–G). Similar results were observed in the transwell assay assessing the invasive capability of tumor cells. After overexpressing COL4A3, the number of melanoma cells migrating to the bottom of the chamber decreased at 24 hours. When COL4A3 was downregulated, the number of cells at the bottom significantly increased compared to the Si-COL4A3 group (Figure 7H–K). These results suggest that modulating COL4A3 can affect the proliferation, migration, and invasion capabilities of A357 and SKMEL28 cells.

Impact of COL4A3 on the Inhibitory Effect of Imatinib on Melanoma Cells

To ascertain whether COL4A3 enhances the anti-tumor efficacy of the small-molecule targeted drug imatinib, the vitality of melanoma cells from different groups was observed after the addition of imatinib at standard concentrations. By

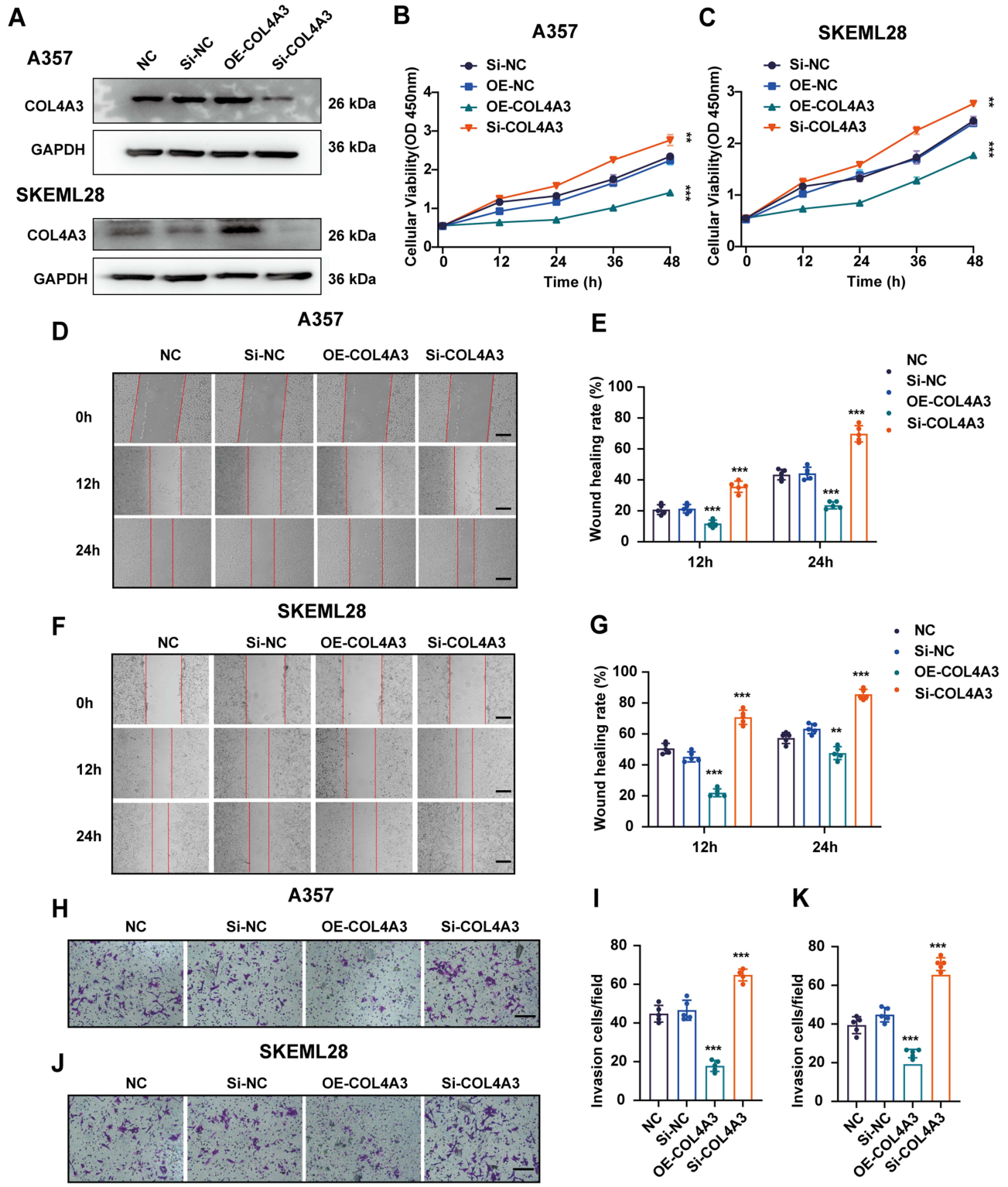

Figure 7 The expression of COL4A3 can impact the vitality of melanoma cells in vitro (**A**) A357 and SKMEL-28 are transfected with Si-NC, Si-COL4A3, and pcDNA3.1-COL4A3 for 24h, and WB detects the expression level of COL4A3. (**B** and **C**) Cell Counting Kit-8 (CCK8) detects A357 and SKMEL-28 viability in all groups at multiple time points (mean ± SEM, n = 5). (**D**–**G**) The migration rate of the A357 and SKMEL-28 in each group were detected using a wound-healing assay (mean ± SEM, n = 3), The scale bar is 100 μm. (**H**–**K**) The invasion ability of the A357 and SKMEL-28 in each group was detected by transwell assay (mean ± SEM, n = 3), The scale bar is 100 μm. *P<0.05, ** P<0.01, ***P<0.001.

detecting apoptosis-related proteins, BCL-2 and Cleaved-Caspase3, it was observed that cells overexpressing COL4A3 exhibited a significant upregulation in the expression levels of BCL-2 and Cleaved-Caspase3 under the influence of imatinib, compared to the group treated with imatinib alone. However, when Si-COL4A3 was used in conjunction with imatinib, the level of apoptosis in the cells was significantly reduced (Figure 8A–F). The results of CCK-8 suggest that overexpression of COL4A3 enhances the inhibitory effect of imatinib on melanoma cell proliferation. Conversely, in the group where COL4A3 was downregulated in combination with imatinib, the results indicate that cell proliferation vitality is significantly higher than in the imatinib-only group (Figure 8G and H). Similar observations were made in the wound healing assay. At 24 hours, overexpression of COL4A3 significantly enhanced the inhibitory effect of imatinib on cell migration, while downregulation of COL4A3 resulted in a significant weakening of imatinib's inhibitory effect (Figure 8I–L). Moreover, the inhibitory effect of imatinib on the migration capability of melanoma cells is enhanced with the overexpression of COL4A3 (Figure 8M–O). These results indicate that modulating COL4A3 can influence the inhibitory effects of imatinib on the proliferation, migration, and invasive capabilities of A357 and SKMEL28 cells.

Discussion

SKCM is distinguished by one of the highest mutation rates among various cancer forms, with family mutation susceptibility playing a significant role in its carcinogenesis.[21] $BRAFV^{600E}$ and $NRASQ^{61R}$ stand out as the most prominent mutant genes, often regarded as the "star" mutations, occurring in 52% and 23% of SKCM patients, respectively.[22] These mutations hold significant clinical value in guiding diagnosis and predicting prognosis. UV is a significant factor contributing to the initiation and progression of SKCM, leading to mutations in both oncogenes and tumor suppressor genes. Previous research indicates that UV radiation induces mutations in TP53/Trp53, significantly enhancing the development and metastasis of $BRAFV^{600E}$-specific mutations in mouse SKCM, ultimately impacting the mice's survival.[23,24] Furthermore, UV-induced DNA toxicity and mutations are irreversible and accumulative. Common cancer driver genes such as TP53 and NF1 exhibit transcriptional regulation by UV-induced reactive oxygen species (ROS), thereby increasing the risk of SKCM occurrence.[25] In summary, UV radiation plays a facilitating role in the metastasis of SKCM, with the induction of frequent gene mutations being one of its primary mechanisms. However, there is currently a lack of research on UV-related cancer genes and their mutation profiles. In this study, we innovatively associated the UV exposure score from clinical features with DEGs related to SKCM progression using WGCNA. Moreover, leveraging the characteristics of gene mutation frequencies in SKCM patient samples, we constructed a prognostic prediction model for patients associated with UV exposure and correlated with mutations.

WGCNA is a bioinformatics analysis method that groups genes with similar expression patterns into a modular gene network and associates them with clinical features of samples.[26] Many researchers have employed this effective bioinformatics analysis tool to select gene modules of interest in cancer studies.[27,28] Based on WGCNA, the gene hub we identified exhibited a strong correlation with UV exposure. Combining this with the characteristics of mutation frequencies, and utilizing LASSO analysis and multiple regression analysis, the prognostic model constructed demonstrated good predictive performance in the TCGA dataset. This affirms the practicality and clinical significance of the model.

Tumor immune infiltration in the tumor microenvironment is a crucial factor influencing tumor growth.[29,30] Existing research suggests that the anti-cancer immune response in the tumor microenvironment is a continuous autocrine loop process, where immune-stimulating chemicals accumulate, enhancing T-cell responses. This loop consists of seven main steps:[31,32]

1. Step 1: Dendritic cell release and capture of tumor antigens;
2. Step 2: dendritic cell release and capture of tumor antigens;
3. Step 3: initiation and activation of the effector T cell response;
4. Steps 4–5: the immune system activation releases relevant chemokines and cytokines, which recruit immune cells to infiltrate the TME, while activated effector T cells migrate and infiltrate the tumor bed;
5. Step 6: recognizing and binding to tumor cells via TCR interaction with major histocompatibility complex class I molecular antigenic peptides;
6. Step 7: targeting and killing tumor cells.

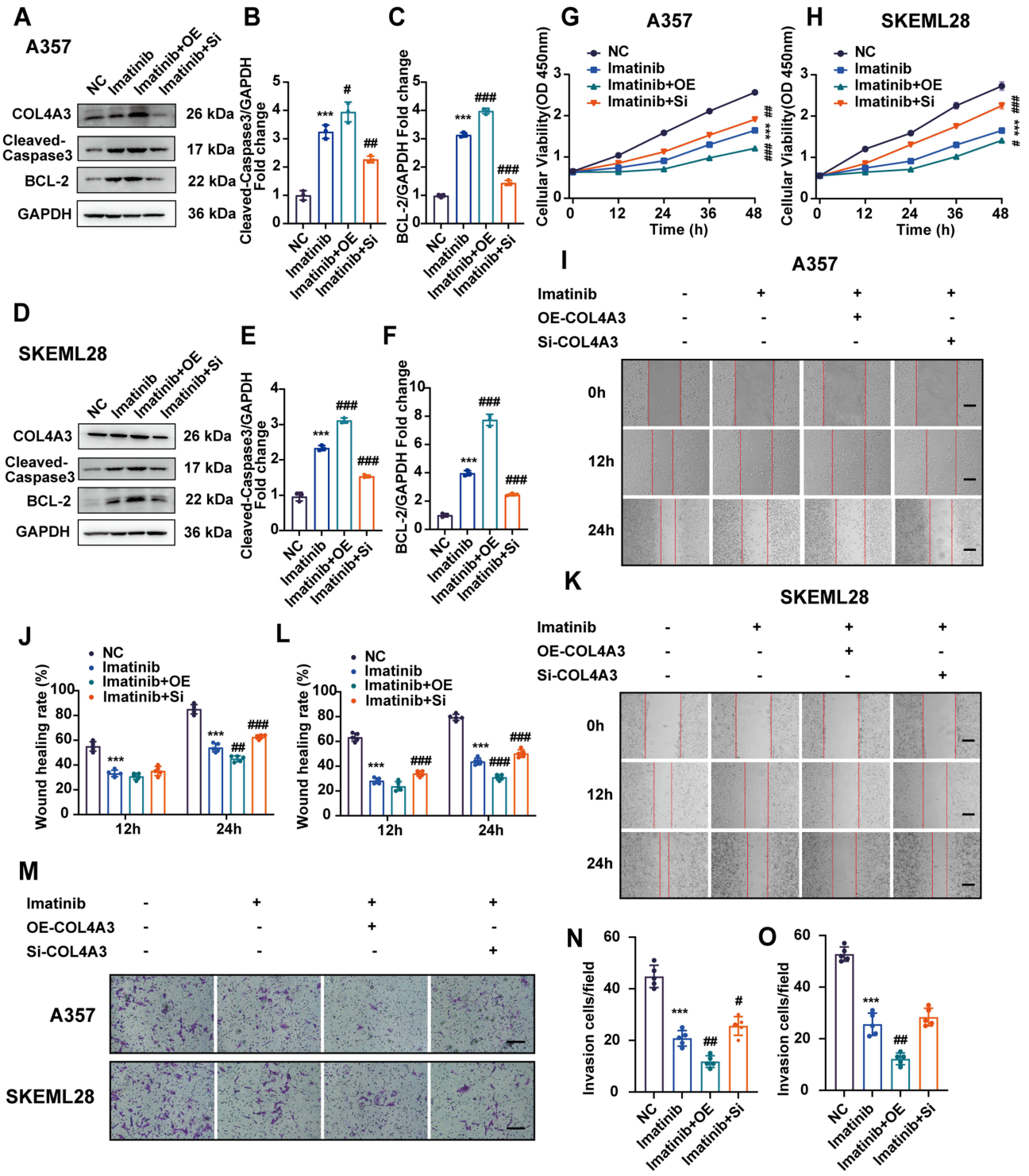

Figure 8 Impact of COL4A3 on the inhibitory effect of imatinib on melanoma cells in vitro (**A-F**) A357 and SKMEL-28 are transfected with Si-COL4A3, and pcDNA3.1-COL4A3 for 24h, followed by imatinib treatment for an additional 24h. And WB detects the expression level of COL4A3, BCL-2, and Cleaved Caspase 3. (**G** and **H**) Cell Counting Kit-8 (CCK8) detects A357 and SKMEL-28 viability in all groups at multiple time points (mean ± SEM, n = 5). (**I–K**) The migration rate of the A357 and SKMEL-28 in each group were detected using a wound-healing assay (mean ± SEM, n = 3), The scale bar is 100 μm. (**M–O**) The invasion ability of the A357 and SKMEL-28 in each group was detected by transwell assay (mean ± SEM, n = 3), The scale bar is 100 μm. **P*<0.05, ** *P*<0.01, ****P*<0.001.

Additionally, killing tumor cells releases more tumor-associated antigens (step 1), expanding and deepening the response in continuous cycles. Almost all 22 types of immune cells participate in this process, especially $CD8^+$ T cells, representing the potential to kill tumor cells to a certain extent.[33] Immune cell types primarily responsible for killing

tumor cells, such as $CD8^+$ T cells and M1-type macrophages involved in antigen presentation, are negatively correlated with the risk score.[34] This indicates that our model can reflect the infiltration level of anti-tumor immune cells in SKCM, indirectly predicting the prognosis of cancer patients. The prognosis model consistently shows a negative correlation with common immune checkpoint inhibitors (ICIs)-related immune checkpoints. This suggests that tumor tissues with high scores exhibit resistance to ICIs treatment, leading to a worsened prognosis for patients.[35]

COL4A3 is one of the genes encoding collagen IV, a major component of the basement membrane. The basement membrane of the skin is a crucial structure between the epidermis and the dermis. Its primary components include collagen IV and collagen VII, which form a meshwork through interactions, creating a structure with tissue connectivity, signaling transduction, and permeability barrier functions.[36] On the contrary, invasive SKCM exhibits distant metastasis due to the upregulation of metalloproteinases. Metalloproteinases degrade the extracellular matrix and disrupt the basement membrane, facilitating the spread of cancer cells to distant locations.[37] Moreover, the expression level of COL4A3 in tumor cells is closely related to the progression of cancer.[38] Previous studies have reported that the expression of COL4A3 in gastric cancer tissues is significantly lower than in matched non-tumor mucosal tissues and positively correlates with the size, lymphatic infiltration, venous infiltration, and TNM staging of gastric cancer.[39] Another study found that in downward progressing nasopharyngeal carcinoma tissues, the expression level of COL4A3 is decreased. The relationship between COL4A3 and the immune microenvironment is closely intertwined, particularly with $CD8^+$ T cells and M1 macrophages. Literature reports indicate that COL4A3, as a key prognostic gene, shows a significant correlation with $CD8^+$ T cells, suggesting its involvement in shaping the immune landscape of breast cancer.[40] Moreover, COL4A3 deficiency correlates with the induction of M1 macrophages, exacerbating intrarenal inflammation and accelerating the progression of Alport nephropathy.[41] Knocking down COL4A3 in nasopharyngeal carcinoma cells significantly enhances cell invasion and migration, thereby promoting the metastasis of nasopharyngeal carcinoma.[42] However, the connection between COL4A3 and SKCM has not been thoroughly investigated. This study discovered that COL4A3 holds a prominent position in the model we constructed, and both its mutation rate and expression level demonstrate the ability to predict patient prognosis.

Imatinib, as an effective targeted therapy for melanoma, exerts its anti-tumor effects by inhibiting specific tyrosine kinases. It plays a role in killing tumor cells and inhibiting tumor invasion and metastasis.[43] The intrinsic molecular mechanisms of Imatinib treatment for SKCM are not fully understood. Some studies indicate that, in addition to BRAF-mutated melanoma, activating mutations in KIT can significantly enhance the efficacy of Imatinib against SKCM.[44] Imatinib can also suppress SKCM proliferation and migration and promote cell apoptosis by inhibiting the expression and activity of the platelet-derived growth factor (PDGF) signaling pathway, leading to downstream Erk signal downregulation.[45] The PI3K/Akt signaling pathway is also one of the classical synergistic pathways of Imatinib. Imatinib effectively inhibits the acetylation of PDGFC, thereby inhibiting the PI3K/AKT signaling pathway and achieving the inhibition of tumor cell proliferation.[46] There is currently no literature reporting the correlation between COL4A3 expression and the efficacy of Imatinib.

Our study has some potential limitations. Firstly, Currently, there is no literature reporting the correlation between UV-induced COL4A3 mutation and mRNA expression level. However, some studies have suggested that the impact of UV-induced mutations on gene RNA expression levels is uncertain, with potential for both up-regulation and down-regulation. Further molecular experiments are warranted to investigate this aspect, and the results should be interpreted in future studies. Moreover, this study was further validated by comparing the groups with knocked-down or overexpressed COL4A3 when combined with Imatinib. Combining the earlier literature suggesting the synergistic relationship between COL4A3 and the PI3K/AKT signaling pathway, we speculate that changes in the PI3K/AKT signaling pathway might be a key factor in the synergistic effect between COL4A3 and Imatinib. However, these hypotheses need further exploration through additional laboratory experiments. In the results of the Transwell assay in the eighth part of this study, we observed that the differences between the group using Si-COL4A3 in combination with Imatinib and the group using Imatinib alone were not significant. We speculate that this may be due to the simultaneous impact of downregulating COL4A3 expression on the expression or activity of metalloproteinases.

Conclusions

In summary, this study identified a gene hub in SKCM that is both associated with UV exposure and characterized by high-frequency mutations. And the construction of a scoring model demonstrated strong predictive capabilities for patient prognosis and tumor immune infiltration. Notably, COL4A3 emerged as an independent risk factor in the model, showing associations with the efficacy of various small-molecule targeted drugs. The in vitro experiments with SKMEL28 and A357 cells provided additional evidence for the crucial role of COL4A3. Based on its mutations and expression levels, COL4A3 stands out as a novel diagnostic and therapeutic target for SKCM, offering new strategies for small-molecule targeted drug therapies.

Data Sharing Statement

The following information was supplied regarding data availability: The dataset of TCGA-SKCM generated and/or analyzed during the current study are available at the TCGA database (https://cancergenome.nih.gov/). The datasets generated and/or analyzed during the current study are available at GEO: GSE59455. The core code of this study has been uploaded to GitHub: https://github.com/Lizhiyongjuan/Code.git. The datasets used and/or analyzed during the current study available from the corresponding author on reasonable request. We declared that materials described in the manuscript, including all relevant raw data, will be freely available to any scientist wishing to use them for non-commercial purposes.

Statement of Ethics

Ethical approval was granted by the ethics committee of the Dongfang Hospital Affiliated to Tongji University School of Medicine with ethics number no. 063 in 2024. The manuscript does not contain experiments using animals and human studies.

Funding

This work was supported by Medical Discipline Construction Project of Pudong Health Committee of Shanghai (Grant No. PWYts2021-07).

Disclosure

The authors declare that they have no known competing financial interests or personal relationships that could have appeared to influence the work reported in this paper.

References

1. Zhu Y, Song B, Yang Z, Peng Y, Cui Z, Chen L and Song B. (2023). Integrative lactylation and tumor microenvironment signature as prognostic and therapeutic biomarkers in skin cutaneous melanoma. J Cancer Res Clin Oncol, 149(20), 17897–17919. doi:10.1007/s00432-023-05483-7
2. Zhao X, Little P, Hoyle AP, et al. The prognostic significance of low-frequency somatic mutations in metastatic cutaneous melanoma. *Front Oncol*. 2018;8:584. doi:10.3389/fonc.2018.00584
3. Hodis E, Watson IR, Kryukov GV, et al. A landscape of driver mutations in melanoma. *Cell*. 2012;150:251. doi:10.1016/j.cell.2012.06.024
4. Sugiyama T, Chen Y. Biochemical reconstitution of UV-induced mutational processes. *Nucleic Acids Res*. 2019;47:6769. doi:10.1093/nar/gkz335
5. Yang Y, Yin R, Wu R, et al. DNA methylome and transcriptome alterations and cancer prevention by triterpenoid ursolic acid in UVB-induced skin tumor in mice. *Molec Carcinogenesis*. 2019;58:1738. doi:10.1002/mc.23046
6. Wang W, Chapman NM, Zhang B, et al. Upregulation of PD-L1 via HMGB1-Activated IRF3 and NF-κB Contributes to UV Radiation-Induced Immune Suppression. *Cancer Res*. 2019;79:2909. doi:10.1158/0008-5472.CAN-18-3134
7. Sreevidya CS, Fukunaga A, Khaskhely NM, et al. Agents that reverse UV-Induced immune suppression and photocarcinogenesis affect DNA repair. *J Invest Dermat*. 2010;130:1428. doi:10.1038/jid.2009.329
8. Ghiasvand R, Robsahm TE, Green AC, et al. Association of phenotypic characteristics and UV radiation exposure with risk of melanoma on different body sites. *JAMA Dermatol*. 2019;155:39. doi:10.1001/jamadermatol.2018.3964
9. Choi H, Yoon JH, Youn K, et al. Decursin prevents melanogenesis by suppressing MITF expression through the regulation of PKA/CREB, MAPKs, and PI3K/Akt/GSK-3β cascades. *Biomed Pharmacoth*. 2022;147:112651. doi:10.1016/j.biopha.2022.112651
10. Di Matteo S, Munari E, Fiore PF, et al. The roles of different forms of IL-15 in human melanoma progression. *Front Immunol*. 2023;14:1183668. doi:10.3389/fimmu.2023.1183668
11. Emmons MF, Faião-Flores F, Sharma R, et al. HDAC8 regulates a stress response pathway in melanoma to mediate escape from braf inhibitor therapy. *Cancer Res*. 2019;79:2947. doi:10.1158/0008-5472.CAN-19-0040
12. Wong KM, King DA, Schwartz EK, et al. Retinoblastoma protein regulates carcinogen susceptibility at heterochromatic cancer driver loci. *Life Sci Alliance*. 2022;5:e202101134. doi:10.26508/lsa.202101134

13. Gao J, Aksoy BA, Dogrusoz U, et al. Integrative analysis of complex cancer genomics and clinical profiles using the cBioPortal. *Sci Signaling*. 2013;6:l1. doi:10.1126/scisignal.2004088
14. Rhodes DR, Kalyana-Sundaram S, Mahavisno V, et al. Mining for regulatory programs in the cancer transcriptome. *Nature Genet*. 2005;37:579. doi:10.1038/ng1578
15. Langfelder P, Horvath S. WGCNA: an R package for weighted correlation network analysis. *BMC Bioinf*. 2008;9:559. doi:10.1186/1471-2105-9-559
16. Subramanian A *et al*. (2005). Gene set enrichment analysis: A knowledge-based approach for interpreting genome-wide expression profiles. Proc. Natl. Acad. Sci. U.S.A., 102(43), 15545–15550. doi:10.1073/pnas.0506580102
17. Lin WP, Xing KL, Fu JC, et al. Development and validation of a model including distinct vascular patterns to estimate survival in hepatocellular Carcinoma. *JAMA network open*. 2021;4:e2125055. doi:10.1001/jamanetworkopen.2021.25055
18. Newman AM, Liu CL, Green MR, et al. Robust enumeration of cell subsets from tissue expression profiles. *Nature Methods*. 2015;12:453. doi:10.1038/nmeth.3337
19. Yang W, Soares J, Greninger P, et al. Genomics of drug sensitivity in cancer (GDSC): A resource for therapeutic biomarker discovery in cancer cells. *Nucleic Acids Res*. 2013;41:D955. doi:10.1093/nar/gks1111
20. Zhao S, Mi Y, Guan B, et al. Tumor-derived exosomal miR-934 induces macrophage M2 polarization to promote liver metastasis of colorectal cancer. *J Hematol Oncol*. 2020;13:156. doi:10.1186/s13045-020-00991-2
21. Liu H, Tang T. Pan-cancer genetic analysis of cuproptosis and copper metabolism-related gene set. *Front Oncol*. 2022;12:952290. doi:10.3389/fonc.2022.952290
22. Calbet-Llopart N, Potrony M, Tell-Martí G, et al. Detection of cell-free circulating BRAF(V) (600E) by droplet digital polymerase chain reaction in patients with and without melanoma under dermatological surveillance. *British j Dermatol*. 2020;182:382. doi:10.1111/bjd.18147
23. Choi YS, Fisher DE. UV and melanoma: the TP53 link. *Cell Res*. 2014;24:1157. doi:10.1038/cr.2014.95
24. Nair S, El-Yazbi AF. Novel genosensor for probing DNA mismatches and UV-induced DNA damage: sequence-specific recognition. *Int J Biol Macromol*. 2023;233:123510. doi:10.1016/j.ijbiomac.2023.123510
25. Melamed RD, Aydin IT, Rajan GS, et al. Genomic characterization of dysplastic nevi unveils implications for diagnosis of melanoma. *J Invest Dermat*. 2017;137:905. doi:10.1016/j.jid.2016.11.017
26. Tan Z, Chen X, Zuo J, et al. Comprehensive analysis of scRNA-Seq and bulk RNA-Seq reveals dynamic changes in the tumor immune microenvironment of bladder cancer and establishes a prognostic model. *J Transl Med*. 2023;21:223. doi:10.1186/s12967-023-04056-z
27. Li YK, Zeng T, Guan Y, et al. Validation of ESM1 related to ovarian cancer and the biological function and prognostic significance. *Int J Bio Sci*. 2023;19:258. doi:10.7150/ijbs.66839
28. Bai M *et al*. (2023). Integrated analysis of EGFR mutated non-small cell lung cancer reveals two distinct molecular subtypes. Clinical & Translational Med, 13(10), 10.1002/ctm2.1431
29. Yang B, Li X, Zhang W, et al. Spatial heterogeneity of infiltrating T cells in high-grade serous ovarian cancer revealed by multi-omics analysis. *Cell Rep Med*. 2022;3:100856. doi:10.1016/j.xcrm.2022.100856
30. Liu L, Zhang Z, Jiang C, Zhu Y, Han R, Wu L and Xu Y. (2024). HOXC9 characterizes a suppressive tumor immune microenvironment and integration with multiple immune biomarkers predicts response to PD-1 blockade plus chemotherapy in lung adenocarcinoma. Aging, 10.18632/aging.205637
31. Y Y, Zhang X. Comprehensive analysis of anoikis-related long non-coding RNA immune infiltration in patients with bladder cancer and immunotherapy. *Front Immunol*. 2022;13:1055304. doi:10.3389/fimmu.2022.1055304
32. Zhang B, Wang Z. A novel pyroptosis-regulated gene signature for predicting prognosis and immunotherapy response in hepatocellular carcinoma. *Front Mol Biosci*. 2022;9:890215. doi:10.3389/fmolb.2022.890215
33. Baharom F, Ramirez-Valdez RA, Khalilnezhad A, et al. Systemic vaccination induces CD8(+) T cells and remodels the tumor microenvironment. *Cell*. 2022;185:4317. doi:10.1016/j.cell.2022.10.006
34. Li Z, Xu W, Yang J, et al. A Tumor microenvironments-adapted polypeptide hydrogel/nanogel composite boosts antitumor molecularly targeted inhibition and immunoactivation. *Advance Mater*. 2022;34:e2200449. doi:10.1002/adma.202200449
35. Liu C, Liu R, Wang B, et al. Blocking IL-17A enhances tumor response to anti-PD-1 immunotherapy in microsatellite stable colorectal cancer. *J Immuno Therap Canc*. 2021;9:e001895. doi:10.1136/jitc-2020-001895
36. Yuan X, Su Q, Wang H, et al. Genetic Variants of the COL4A3, COL4A4, and COL4A5 genes contribute to thinned glomerular basement membrane lesions in sporadic IgA nephropathy patients. *J Amer Socie Nephrol*. 2023;34:132. doi:10.1681/ASN.2021111447
37. Peng K, Zhang Y, Liu D, et al. MMP2 is a immunotherapy related biomarker and correlated with cancer-associated fibroblasts infiltrate in melanoma. *Can Cell Inter*. 2023;23:26. doi:10.1186/s12935-023-02862-5
38. Nie XC, Wang JP, Zhu W, et al. COL4A3 expression correlates with pathogenesis, pathologic behaviors, and prognosis of gastric carcinomas. *Human Pathol*. 2013;44:77. doi:10.1016/j.humpath.2011.10.028
39. Zeng X, Wang HY, Wang YP, et al. COL4A family: potential prognostic biomarkers and therapeutic targets for gastric cancer. *Transl Cancer Res*. 2020;9:5218. doi:10.21037/tcr-20-517
40. Tao D, Wang Y, Zhang X, et al. Identification of angiogenesis-related prognostic biomarkers associated with immune cell infiltration in breast cancer. *Front Cell Develop Biol*. 2022;10:853324. doi:10.3389/fcell.2022.853324
41. Ryu M, Kulkarni OP, Radomska E, et al. Bacterial CpG-DNA accelerates Alport glomerulosclerosis by inducing an M1 macrophage phenotype and tumor necrosis factor-α-mediated podocyte loss. *Kidney Int*. 2011;79:189. doi:10.1038/ki.2010.373
42. Yang X, Wu Q, Wu F, et al. Differential expression of COL4A3 and collagen in upward and downward progressing types of nasopharyngeal carcinoma. *Oncol Lett*. 2021;21:223. doi:10.3892/ol.2021.12484
43. Yan C, Zhao C, Yang K, et al. Rare c-KIT c.1926delA and c.1936T>G mutations in exon 13 define imatinib resistance in gastrointestinal stromal tumors and melanoma patients: Case reports and cell experiments. *Front Mol Biosci*. 2022;9:730213. doi:10.3389/fmolb.2022.730213
44. Berestjuk I, Lecacheur M, Carminati A, et al. Targeting Discoidin Domain Receptors DDR1 and DDR2 overcomes matrix-mediated tumor cell adaptation and tolerance to BRAF-targeted therapy in melanoma. *EMBO Mol Med*. 2022;14:e11814. doi:10.15252/emmm.201911814
45. Thijssen VL, Paulis YW, Nowak-Sliwinska P, et al. Targeting PDGF-mediated recruitment of pericytes blocks vascular mimicry and tumor growth. *J Pathol*. 2018;246:447. doi:10.1002/path.5152
46. Damsky WE, Curley DP, Santhanakrishnan M, et al. β-catenin signaling controls metastasis in Braf-activated Pten-deficient melanomas. *Cancer Cell*. 2011;20:741. doi:10.1016/j.ccr.2011.10.030